scientific reports

Check for updates

OPEN

Identification of new selective CD36 inhibitors to potentiate HER2-targeted therapy in HER2-positive breast cancer

Lorenzo Castagnoli[1,8], Francesco Bonì[2,8], Martina Bigliardi[1], Paolo Toneguzzo[1], Paola A. Corsetto[3], Giorgia Galasso[1], Alma Franceschini[1], Paolo Cocomazzi[2], Viola Regondi[1], Cristian Capuzzoni[1,4], Angela M. Rizzo[3], Francesca Ligorio[5,6], Claudio Vernieri[5,6], Pierfausto Seneci[7], Daniela Arosio[4], Elda Tagliabue[1], Eloise Mastrangelo[2], Mario Milani[2,8]✉ & Serenella M. Pupa[1,8]✉

HER2 overexpression/amplification (HER2+) occurs in approximately 15–20% of breast cancer (BC) and identifies a highly aggressive BC subtype. The cure rate of HER2 + BC has been significantly increased through recent clinical achievements; however, a non-negligible proportion of patients still either fails to respond or acquires resistance to targeted therapies, highlighting the need for novel treatment strategies. As demonstrated in robust preclinical studies, HER2 + BC is considered a neoplastic disease with a peculiar lipogenic phenotype, due to its crucial addiction to an exacerbated need for fatty acids (FAs) produced via FA synthase (FASN), the central lipogenic enzyme required for intracellular de novo FA biosynthesis. FASN is overexpressed/activated in most HER2 + BC cells sustaining their growth, proliferation, and aggressiveness through a reciprocal direct interplay with the HER2-driven oncogenic signaling. Recent evidence shows that rewiring of lipid metabolism in the presence of pharmacological HER2 inhibition impairs FASN up-regulation and activates the compensatory lipid metabolic pathway of FA uptake via the altered expression/activity of the transmembrane CD36 FA transporter. Thus, the latter is emerging as a potentially new and targettable mechanism of resistance to anti-HER2 therapies. Due to the limited availability of drug-like compounds that selectively target CD36, in this study we screened a library of commercial compounds through in silico docking on the crystal structure of the CD36 extracellular domain. We evaluated their chemical-physical, biological and metabolic properties through microscale thermophoresis and molecular dynamics analyses, cell viability assays performed in monotherapy and dual blockade, and gas chromatography-flame ionization detector and BODIPY C16 uptake analyses. Among the best ranked compounds, we selected two promising hits with micromolar affinity for CD36, showing in vitro that they decrease per se the proliferation of HER2 + BC cells resistant to anti-HER2 agents, induce apoptotic effects, significantly reduce FA intracellular internalization, and potentiate the cytotoxic activity of lapatinib, i.e. the most suitable anti-HER2 drug used in in vitro bioassays. Taken together, these findings support that our novel anti-CD36 small molecules should undergo hit-to-lead optimization to prospectively improve the efficacy of anti-HER2 agents in HER2 + BC refractory to targeted therapy.

Keywords Breast cancer, HER2, CD36, Fatty acid uptake, Drug resistance, Drug discovery technologies, Small molecule leads

[1]Microenvironment and Biomarkers of Solid Tumors, Department of Experimental Oncology, Fondazione IRCCS Istituto Nazionale dei Tumori di Milano, Via Amadeo 42, 20133 Milan, Italy. [2]Biophysics Institute, CNR-IBF, Via Corti 12, 20133 Milan, Italy. [3]Department of Pharmacological and Biomolecular Sciences "Rodolfo Paoletti", Università di Milano, Milan, Italy. [4]Istituto di Scienze e Tecnologie Chimiche 'G. Natta' (SCITEC), Consiglio Nazionale delle Ricerche, Via C. Golgi 19, 20133 Milan, Italy. [5]Medical Oncology Department, Fondazione IRCCS Istituto Nazionale dei Tumori, Milan, Italy. [6]AIRC Institute of Molecular Oncology, IFOM ETS, Milan, Italy. [7]Department of Chemistry, Universita' degli Studi di Milano, Via C. Golgi 19, 20133 Milan, Italy. [8]Lorenzo Castagnoli, Francesco Bonì, Mario Milani and Serenella M. Pupa contributed equally to this work. ✉email: mario.milani@cnr.it; Serenella.Pupa@istitutotumori.mi.it

Abbreviations

APC	Allophycocyanin conjugate
ATCC	American Type Culture Collection
BC	Breast cancer
BHT	2,6-bis(1,1-dimethylethyl)-4-methylphenol
C16	Palmitate
CO_2	Carbon dioxide
ΔG	Gibbs free energy. DMEM, Dulbecco's modified Eagle's medium
DMEM	Dulbecco's modified Eagle's medium
DMSO	Dimethyl sulfoxide
DTT	Dithiothreitol
FA	Fatty acid
FASN	Fatty acid synthase
FAT	FA translocase
FBS	Fetal bovine serum
FI	Fold increase
FITC	Fluorescein Isothiocyanate conjugate
GC-FID	Gas chromatography-flame ionization detector
HER2+	HER2 overexpression
Kd	Dissociation constant
LCFAs	Long chain FAs
MD	Molecular dynamics
MST	Microscale thermophoresis
N/A	Not assessed
NPT	Isobaric-isothermal ensemble
NVT	Canonical ensemble
OD	Optical density
ox-LDL	Oxidized low-density lipoprotein
PBS	Phosphate buffer solution
PFL	Positive feedback loop
rMFI	Relative median fluorescence intensity
RPMI1640	Roswell Park Memorial Institute medium
SD	Standard deviation
SEM	Standard error of the mean
SRB	Sulforhodamine B
SSO	Sulfo *N*-succinimidoyl oleate
TKI	Tyrosine kinase inhibitor

Breast cancer (BC) is the most commonly diagnosed malignancy in women worldwide[1]. HER2 overexpression (HER2+) occurs in approximately 15–20% of BCs and is related to high proliferation rate and elevated metastatic potential[2]. In the last two decades, the treatment of HER2 + BC has been revolutionized by the introduction of drugs targeting HER2, resulting in consistent improvement in limited stage and advanced disease outcomes[2]. However, a non-negligible number of surgically treated HER2 + BCs recurs due to primary or acquired resistance to specific HER2 inhibitors, and novel therapeutic strategies are urgently needed. Several intrinsic tumor resistance mechanisms, such as HER2 somatic mutations, expression of truncated receptor variant as p95HER2, constitutive activation of other members in the HER receptor family, hyperactivation of HER2 downstream signaling cascades as PI3K/AKT/mTOR, or the activation of signaling pathways that bypass HER2 inhibition, have been identified[3]. In this context, the reprogramming of lipid metabolism, a well-established hallmark of cancer[4] that plays a key role in carcinogenesis and survival, providing cancer cells with fuel to sustain increased energetic and biosynthetic demands essential for their growth and progression[5,6], has been recently reported as the last frontier among the described mechanisms of HER2 + BC resistance to the specific tyrosine kinase inhibitor (TKI) lapatinib[7]. In particular, the overexpression/activation of Fatty Acid Synthase (FASN), an anabolic enzyme required to catalyze the last step of *de novo* biosynthesis of FAs, represents the most frequent lipid metabolic alteration in the majority of human malignancies. Of note, FASN is overexpressed/activated in 85% of HER2 + BC cases and it is associated with poor clinical outcome[8–10]. Solid preclinical evidence points to the existence of a positive feedback loop (PFL) of reciprocal stimulation/interplay between HER2 and FASN, which couples lipid biosynthesis with oncogenic proliferation pathways, linking energy anabolism with HER2-driven malignant transformation/aggressiveness and metastasis[9,10]. This PFL strongly implies that HER2 inhibition could also be sufficient per se to inhibit FASN, thus promoting HER2 + BC cells to evolve towards compensatory metabolic pathways to guarantee their supply of FA. Enhanced FA uptake via the upregulation of the CD36 receptor is common in human malignancies, and has been implicated in cancer development, growth, aggressiveness, stemness and therapeutic resistance in patients with different oncotypes[11–17]. Indeed, the CD36 receptor, also known as FA translocase (FAT), originally identified as a highly glycosylated transmembrane protein (platelet integral membrane glycoprotein IV), is involved in the intracellular internalization of long-chain FAs (LCFAs)[18], thus supporting the energy production of cancer cells by enhancing lipid uptake and FA β-oxidation[19,20]. Recently, Feng and coauthors reported that CD36 overexpression may represent a compensatory mechanism that helps HER2 + BC cells to escape lapatinib inhibition[21]. In this context, our group showed that high-CD36 gene expression evaluated at baseline predicts poorer long-term clinical outcomes in early-stage HER2 + BC patients treated with neo-adjuvant trastuzumab-based therapy[16]. Very recently, we also demonstrated

that CD36 targeting might be an effective metabolism-based therapeutic strategy in the treatment of this malignancy potentiating anti-HER2 specific drug efficacy by inactivating mesenchymal HER2 + cancer stem cells, i.e. those refractory to any anti-tumor treatment[22]. Of note, lately, in another oncological context, Tzeng and Yu provided evidence that their in-house generated humanized anti-CD36 antibody PLT012, administered with standard liver cancer therapies, effectively enhanced their anti-hepatocellular carcinoma response, leading to consistent tumor growth inhibition and promoting a shift from immunosuppressive to immunoprotective tumor microenvironment[23]. Altogether, these reported findings support the increasingly significant role of CD36 as a new validated metabolic biotarget for the development of novel, more effective anticancer therapies.

Up to now, drug-like CD36 inhibitors suitable for clinical use are still lacking, underscoring the need for the design of better CD36 drug candidates. Indeed, along with different anti-CD36 neutralizing monoclonal antibodies as JC63.1 and FA 6.152 reported to impair the growth of PTEN-/- prostate cancer[24] and to prevent metastasis in preclinical models of human melanoma, breast cancer-derived tumors and oral cancer[13,17], and the recently reported humanized PLT012 antibody reported "to rejuvenate" antitumor immunity in preclinical setting of liver cancer and liver metastasis[23], sulfo-*N*-succinimidyl oleate (SSO)[20] is a known, largely used inhibitor of CD36. Although poorly bioavailable, SSO is a commercial agent with proven pre-clinical efficacy to impair FA uptake through CD36 inhibition[13,20]; however, it was recently suggested that SSO activity is not due to the direct inhibition of CD36, but rather to a general non-specific alteration of intracellular metabolism[25,26]. More recently, the small molecule SMS121 has been shown to bind CD36 with high affinity (Kd ~ 6 μM) and to inhibit FA internalization in acute myeloid leukemia cells (IC50 ~ 160 μM)[27] .

The lack of specific CD36 inhibitors for clinical use represents a major limitation to evaluate if its impairing/inhibition can enhance efficacy of current treatment options, not only for HER2 + BC resistant to target therapy but also for other oncotypes addicted to CD36-mediated FA uptake for their development, proliferation, aggressiveness and metastasis[28].

In this work, to identify more effective and selective CD36 drug-like small molecules, we performed an in silico docking search on the crystal structure of the extracellular domain of CD36[29] using a library of commercially available compounds (https://www.hit2lead.com). The best predicted CD36 interactors were analyzed using different in vitro experimental approaches, which allowed us to select two promising hit compounds **11** and **13**. Our results provide evidence that such hits decrease per se the viability of HER2 + BC cells expressing high levels of CD36, mediate apoptotic effects, affect FA tumor cell internalization, and potentiate the therapeutic activity of lapatinib.

Our preliminary findings pave the way for developing novel FA uptake-targeted therapeutic strategies, that might be used alone or in combination with anti-HER2 compounds to potentiate the efficacy of current options for HER2 + BC patients resistant to target therapy.

Materials and methods

In silico docking

The crystal structure of CD36[29] was modified by adding hydrogen atoms and Kollman charges (*AutoDockTools* and *Python Molecular Viewer;* https://ccsb.scripps.edu). A protein region around the FA binding cavity centered at Val142, with 33.8 × 33.8 × 33.8 $Å^3$dimensions, was selected for in silico analysis of a library of 30,000 compounds (ChemBridge Corp, https://www.hit2lead.com). The analysis was primarily performed using *AutoDock Vina*[30] to extract the 113 best compounds, subsequently subjected to an additional screening with *AutoDock4.2*[31] (Lamarckian genetic algorithm (ga): num_evals = 1750000, pop_size = 150, run = 80), identifying the best ligands in the library.

Microscale thermophoresis analysis of the selected compounds

Recombinant CD36 protein was purchased from MedChemExpress (MCE® Monmouth Junction, NJ, USA). CD36 (12 μM concentration) was labeled to Lys residues (NHS-2nd Generation Labeling Kit; Nanotemper Technologies), and purified in phosphate buffer solution (PBS; pH 7.4) at a final concentration of 2 μM and a 73% degree of labeling. Microscale thermophoresis (MST) experiments were performed on a Monolith NT.115 instrument (Nanotemper Technologies, Munich, Germany). Samples were prepared by adding 80 nM of labeled CD36 to an equal volume of serial dilutions of each ligand [4% dimethyl sulfoxide (DMSO)] with 60% excitation and medium MST power.

When a ligand-induced change in the initial fluorescence was observed, the change was analyzed with a standard deviation test (*SD-test*) to verify that it resulted from the interaction between the ligand and the labeled protein in its native state. For the SD test, samples without/with the ligand (1 mM) were centrifuged for 10 min at 15,000 × g, denatured at 95 °C for 5 min after the addition of 2xSD mixture (4% SDS, 40 mM DTT), and measured.

Tumor cell lines

Human HER2 + BC cell lines MDAMB361[32], HCC1569[33,34], EFM192A and BT474 with different sensitivity to anti-HER2 drugs[34] were purchased from American Type Culture Collection (ATCC; Rockville, MD, USA). MDAMB361 and BT474 cells were grown in monolayer cultures in DMEM (EuroClone, Pero, MI, Italy) supplemented with 10% fetal bovine serum (FBS) (Sigma-Aldrich, St. Louis, MO, USA), whereas EFM192A and HCC1569 cells were grown in monolayer cultures in RPMI 1640 medium (EuroClone) supplemented with 10% FBS.

Tumor cell lines were cultured at 37 °C in a humidified 5% CO_2 atmosphere, and routinely tested for mycoplasma contamination using the MycoAPe Plus Kit (Lonza, Basel, Switzerland). The MDAMB361 and BT474 tumor cell lines were obtained between 2000 and 2012, and were authenticated by short tandem repeat

DNA fingerprinting (Eurofins Genomics, Louisville, KY, USA; last verification, 2022). HCC1569 and EFM192A cell lines were purchased from ATCC in 2021.

Flow cytometry analysis

MDAMB361, HCC1569, EFM192A and BT474 HER2 + BC cell lines were incubated for 1 h at 37 °C with an allophycocyanin (APC)-conjugated anti-human CD36 antibody [clone: 5-271, (BioLegend, San Diego, CA, USA)] to analyze CD36 expression with a matched/corresponding isotype control APC Mouse IgG2a κ antibody in the dark at 4 °C for 30 min (BioLegend). Unbound antibodies were removed with staining buffer, and cells were analyzed using a BD LSR II FACSCanto cytometer (BD Biosciences, Franklin Lakes, NJ, USA). The collected events were analyzed using FlowJo software v10.10 (BD Life Sciences; https://flowjo.com). The relative mean fluorescence intensity (rMFI) was determined by gating on live cells and subtracting the background (isotype) MFI. In all experiments, data were processed using the FlowJo software package.

BODIPY™ FL C16 (4,4-Difluoro-5,7-Dimethyl-4-Bora-3a,4a-Diaza-s-Indacene-3-Hexadecanoic Acid) uptake assay

The FA uptake assay was performed as previously described[35]. Briefly, screened MDAMB361, HCC1569, EFM192A and BT474 cell lines expressing different levels of CD36 were seeded at a 4×10^5 density in a 6-well plate for 72 h before the experiments. Cells were cultured in serum-free media supplemented with 2 µM BODIPY FL C16 (Thermo Fisher Scientific, Waltham, MA, USA) for 30 min at 37 °C. After washing, cells were harvested and analyzed by flow cytometry. The MFI was compared between samples and the internal control.

Sulforhodamine B (SRB) cell viability/proliferation assay

HCC1569 and MDAMB361 cell lines expressing higher levels of CD36, and BT474 cells expressing very low levels of CD36 were selected for the cytotoxic bioassays and seeded in 96-well plates at a $3–5 \times 10^3$ density per well for 72 h before incubation for different time intervals (48 h, 72 h and 96 h) with the proper concentrations of putative anti-CD36 interactors (12.5 µM, 25 µM, 50 µM) diluted in DMSO (see Table 1). DMSO and SSO, tested at 50 µM and 100 µM, were used as internal controls for the antitumor activity exerted by each compound.

Lapatinib alone, tested at 7.2 µM, or in combination with selected hits **11** and **13** (12.5 µM and 25 µM) was used to evaluate the percentage of cell viability following different treatments. Tumor cell proliferation was assessed using the SRB assay, as previously reported[36]. Briefly, after each incubation period, cell monolayers were fixed with 10% trichloroacetic acid and stained with SRB for 30 min. The excess dye was then removed by repeated washings with 1% acetic acid, after which the protein-bound dye was dissolved in 10 mM Tris solution for optical density (OD) determination at 564 nm. The number of living cells is proportional to the amount of solubilized dye. Cell proliferation inhibition (%) was calculated as {(untreated - treated)/(untreated)}X100 and plotted using GraphPad Prism 5.02.

Caspase-3 activity

To evaluate the apoptotic activity mediated by **11** and **13** in CD36-expressing HCC1569 and MDAMB361 cells, the Caspase-Glo 3/7 3D assay (Promega, Madison, WI) was used following the manufacturer's instructions. Specifically, cells were first seeded in 96-well plates at a 20,000 cell density per well for 72 h before the addition of either selected anti-CD36 inhibitors **11** and **13** tested at 25 µM and 50 µM, or DMSO as an internal control. After incubation for different time intervals (48 h, 72 h and 96 h), the Caspase-Glo 3/7 3D assay reagent was added to each well. Plates were subsequently covered and gently mixed at room temperature for 30 min on a plate shaker, then luminescence was detected through a Spark multimode microplate reader (Tecan, Männedorf,

Cpd	Molport code	In silico ΔG (kcal/mol)	DMSO solubility (mM)	in vitro Kd (µM)
1	002-247-404	− 10.5	< 5	N/A*
2	002-513-115	− 11.1	< 5	N/A
3	001-990-359	− 10.6	25	N/A
4	000-786-030	− 11.2	5	N/A
5	002-216-734	− 10.6	25	No binding
6	000-665-428	− 10.6	10	No binding
7	000-729-748	− 10.6	10	N/A
8	001-989-163	− 10.7	10	> 1000
9	002-228-689	− 10.8	5	N/A
10	002-047-460	− 10.8	10	N/A
11	002-127-661	− 10.1	25	20 ± 7
12	002-253-463	− 10.3	25	No binding
13	002-233-680	− 10.3	25	10 ± 4
14	000-836-502	− 11.0	< 5	N/A
15	000-749-803	− 10.4	10	No binding

Table 1. Computational and experimental characterization of the top 15 CD36 ligands identified through molecular docking. *N/A not assessed.

Switzerland). Caspase-3/7 activity (%) was calculated as {(untreated − treated)/(untreated)} × 100 and plotted using GraphPad Prism 5.02.

Gas chromatography-flame ionization detector (GC-FID) analysis

HCC1569 and MDAMB361 cell lines were seeded at a 4×10^5 density in a 6-well plate and left to adhere for 72 h. BC cells were exposed to 50 µM palmitic acid (C16:0) in the presence or absence of **11** or **13** (25 µM) for 60 min. Untreated cells not exposed to any exogenous FA but to an equal concentration of DMSO, or **11** or **13** hits, were also included. Lipids from HCC1569 and MDAMB361 pellets were extracted using a slightly modified Folch method[37]. The medium used in this study contained 50 µM 2,6-bis(1,1-dimethylethyl)-4-methylphenol (BHT) to protect lipids from oxidation. Before lipid analysis, dried organic layers were reconstituted in chloroform: methanol (2:1, vol/vol). Total FAs were determined as methyl esters by gas chromatography. FA methyl esters were obtained by reaction with 3.33% (w/v) sodium methoxide in methanol and injected into a capillary gas chromatograph (Shimadzu GC-2025) equipped with a flame ionization detector. Their separation was achieved using the following parameters: capillary Zebron FAME, length 30 m x 0.25 mm I.D., film thickness 0.20 µm; carrier gas, helium; injector temperature, 250 °C; detector temperature, 275 °C; and oven temperature, 100 °C for 2 min and then increased to 250 °C at 10 °C min^{-1} rate. A standard mixture containing all FA methyl esters was injected for calibration, and the triglyceride C17:0 was used as an internal standard[38].

Molecular dynamics (MD)

Two MD simulations were performed with the program GROMACS[39] using the GROMOS96 54a7 force field[40]adding to CD36 (PDB-ID 5LGD[29,41] a molecule of **11** or **13**, placed in its best pose from the in silico docking search.

Hits **11** and **13** were parametrized with *Automated Topology Builder ATB3.0* (https://atb.uq.edu.au/; molid = 1573429/1573431)[41].

For **11**/**13**, the parallelepipedal box for the simulation was filled with 15,724/15,721 water molecules, and the system charge (+1) was equilibrated with 20 and 21 atoms of Na^+ and Cl^-, respectively. After minimization with the steepest descent algorithm (final potential energy = -8.56/8.57e + 05 kJ mol^{-1}), we performed two equilibrations, each lasting for 2 ns, in the NVT ensemble at T = 100 K and T = 300 K.

Each productive run (250 ns) was performed in the NPT ensemble at atmospheric pressure with Particle Mesh Ewald for long-range electrostatics, a 2 fs time step (leap-frog integrator), T-coupling with a modified Berendsen thermostat and P-coupling Parrinello-Rahman, with periodic boundary conditions.

Statistical analysis

All statistical analyses were conducted with GraphPad Prism 5.02 software, using unpaired or paired two-tailed Student's t tests as appropriate. When $p < 0.05$, the difference between compared groups was considered statistically significant. Data are presented as the mean ± standard error of the mean (SEM) ($n \geq 3$ biological replicates). The sample size of each individual experiment is reported in the corresponding figure legends.

Results

In silico analysis to identify new CD36 inhibitors

To identify new CD36 inhibitors, we screened in silico a commercial library of 30,000 compounds (https://www.hit2lead.com) targeting a protein region around the FA binding site centered at Val142 (pdb-id: 5LGD chain A[29]. The in silico screening was divided into two runs: first, a fast procedure was used to select the 113 best compounds[30]with predicted binding free energy values (ΔG) ranging from − 10.2 to − 8.9 kcal/mol, which were then subjected to a more accurate analysis with *AutoDock4.2* [31]. The 15 predicted best binders [**1** to **15**, with calculated ΔG values ranging from − 11.2 to − 10.4 kcal/mol and predicted Kd values ranging from 6.3 to 25.3 nM; (Table 1; Supplemental Fig. S1)] were purchased from MolPort (https://www.molport.com/).

The selected compounds **1** to **15** mostly contained two or more hydrophobic aromatic rings systems connected by flexible linker(s); their binding affinity to the chosen cavity of CD36 mostly resulted from hydrophobic interactions, as expected considering the nature of the binding site suitable for hosting lipophilic FAs. In addition to hydrophobic interactions, putative hits established few hydrogen bonds with CD36, mainly involving the side chains of Lys334, Arg337, and Tyr149 and the main chains of Val194, Gly199 and Thr195.

Binding affinity of selected virtual hits to recombinant CD36

Considering the results from in silico docking, we used MST to experimentally assess the binding affinity of 15 selected hit compounds to recombinant CD36, as described in the "Materials and methods" section. Unfortunately, eight compounds could not be tested due to aggregation problems in water (**1**, **2**, **3**, **4**, **7**, **9**, **10**, **14**); compounds **5**, **6**, **12** and **15** did not confirm binding to the protein, whereas **8** showed a weak dissociation constant (Kd) > 1 mM. In contrast, putative hits **11** and **13** bound CD36 with Kd values of 20 ± 7 µM and 10 ± 4 µM, respectively (Fig. 1). For comparison, we also analyzed the known CD36 inhibitor SSO[13,20], that displayed a poorer binding affinity [Kd of 50 ± 10 µM; (Fig. 1)].

Biological properties of HER2 + BC cell lines and antiproliferative activity of selected compounds

To investigate the effect of selected anti-CD36 compounds on HER2 + BC cells, we initially evaluated through flow cytometry analysis the expression of CD36 in lapatinib-resistant HCC1569 and MDAMB361, and lapatinib-sensitive EFM192A and BT474 cell lines, respectively[32–34].

HCC1569 and MDAMB361 showed the higher percentage of CD36 + cells (80%) versus EFM192A (20%) and BT474 cells (Fig. 2A), and higher CD36 levels were observed in HCC1569 and MDAMB361 versus EFM192A

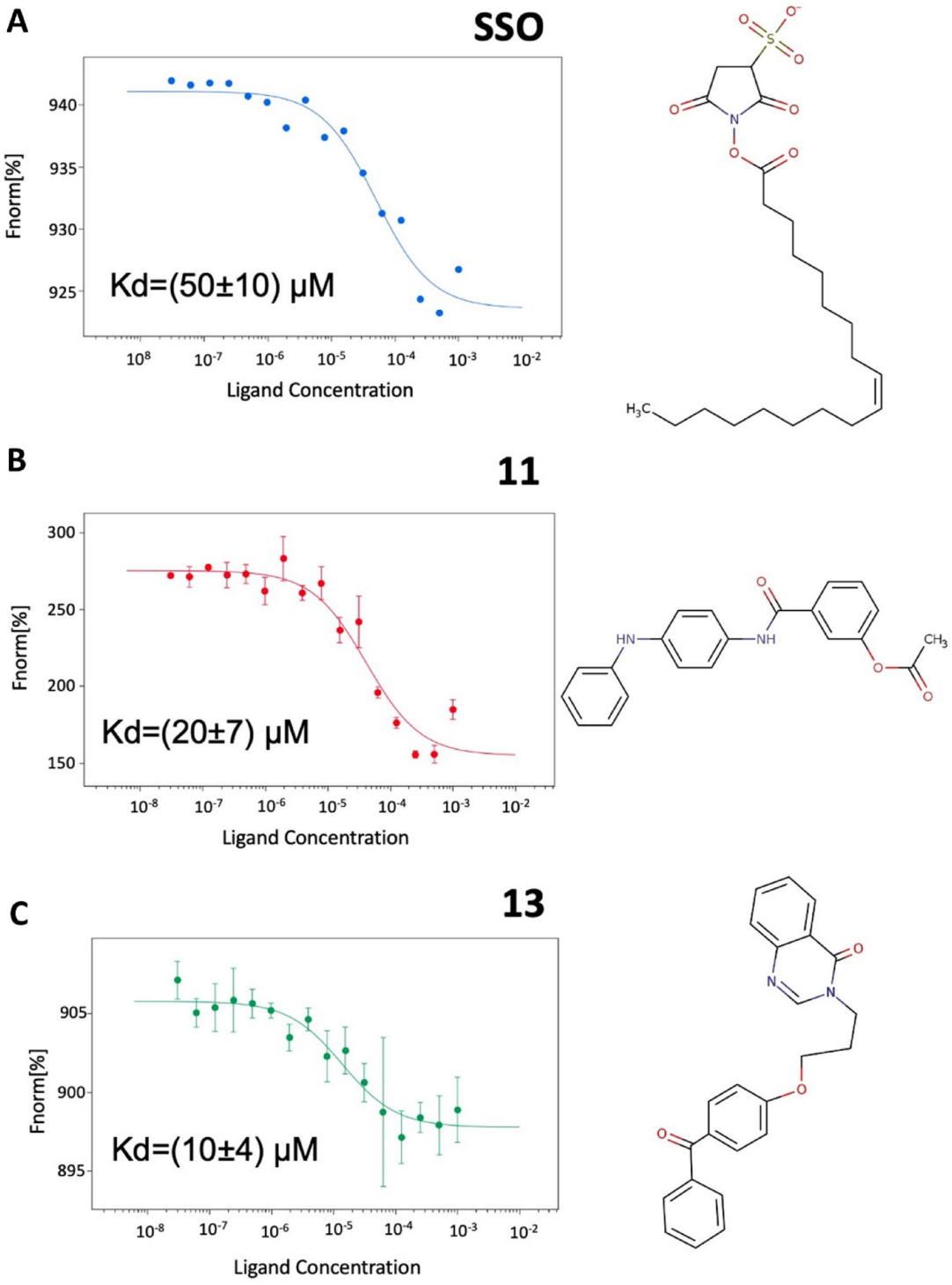

Fig. 1. MST experiments to analyze the binding affinity of (**A**), SSO; (**B**), hit **11;** and (**C**), hit **13** for CD36. Error bars resulted from 3 or 4 independent measures for **11** or **13**, respectively.

and BT474 cells, the latter included as a CD36-negative cell model (Fig. 2A,B). In line with CD36 expression levels, we found that HCC1569 and MDAMB361 cells demonstrated the higher capability to internalize palmitate (C16, green fluorescent BODIPY) versus EFM192A and, above all, BT474 cells (Fig. 2C). According to these data, HCC1569 and MDAMB361 cells were selected as the most suitable targets to proceed with the biological profiling of all putative CD36 binders.

Twelve of the 15 compounds (**1**, **2** and **14** were not tested due to their poor DMSO solubility) were incubated for 96 h with HCC1569 and MDAMB361 cells at 25 μM or 50 μM concentrations, to investigate their effects on cell viability via SRB assay. We observed that **4**, **6**, **7**, **8**, **9**, **10**, **12** and **15** did not exert any significant cytotoxic

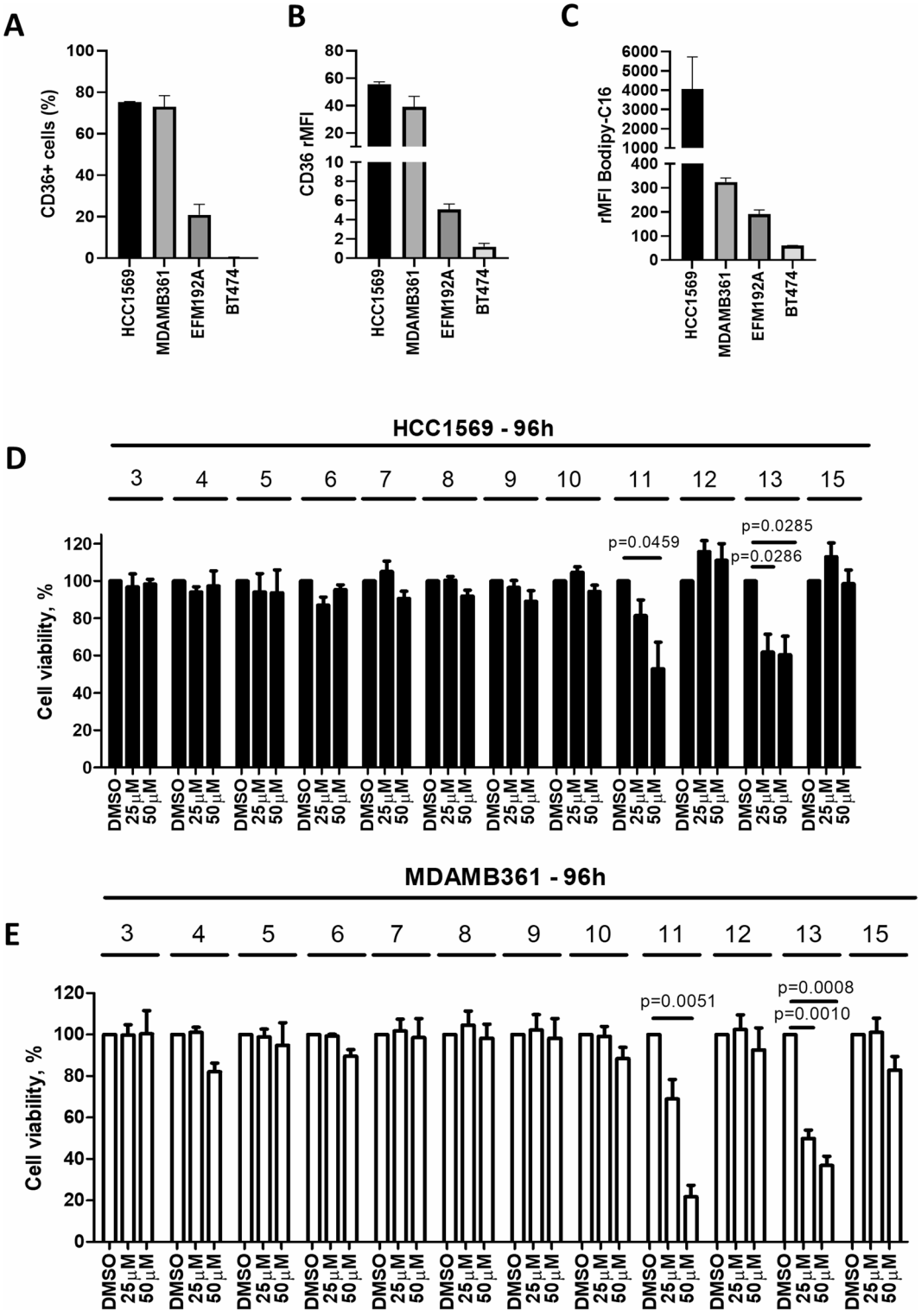

Fig. 2. Biological features of HER2 + BC cells and cytotoxic activity of putative virtual hits. (**A**) Percentage (%) of CD36 + cells in HER2 + BC cell lines HCC1569, MDAMB361, EFM192A and BT474 evaluated by flow cytometry analysis; (**B**) CD36 relative median fluorescence intensity (rMFI) of HER2 + BC cell lines HCC1569, MDAMB361, EFM192A and BT474 evaluated by flow cytometry analysis; (**C**) Analysis of FA uptake in HCC1569, MDAMB361, EFM192A and BT474 cells incubated with fluorescent Bodipy-C16 assay for 30 min evaluated by Bodipy FL C16 uptake assay; (**D**) Tumor proliferation of HCC1569 and (**E**) MDAMB361 cells upon exposure for 96 h to 25 µM and 50 µM of putative anti-CD36 inhibitors **3**, **4**, **5**, **6**, **7**, **8**, **9**, **10**, **11**, **12**, **13**, and **15** evaluated by an SRB bioassay. Values were normalized to the growth of the cells incubated with DMSO. The data are presented as the means ± SEMs ($n = 3$). Significance was calculated by using a two-tailed paired Student's t test.

effect on treated cells, whereas **11** and **13**, both with significant affinity for CD36 (Fig. 1), decreased tumor cell growth (Fig. 2D,E), and were therefore selected for further analysis.

Hits 11 and 13 exert cytotoxic activity and cause cell death in HER2 + BC cells

To assess whether the different affinities of **11**, **13** and SSO for CD36 (Fig. 1) were correlated with their capability to affect HCC1569, MDAMB361 and BT474 (negative control) cell viability, we tested their cytotoxic activity at different time intervals (48 h, 72 h and 96 h) and at different concentrations (12,5; 25 and 50 μM). As shown in Fig. 3A,B, incubation with SSO (up to 100 μM) did not affect tumor proliferation on the three tested cell lines. Conversely, **11** and **13** negatively affected the viability of HCC1569 and MDAMB361 cells at all tested concentrations, and at every time point compared with the BT474 cell control (Fig. 3A,B).

The ability of **11** and **13** to mediate cell death via induction of apoptosis was then measured using the commercial Caspase-Glo 3/7 3D assay in HCC1569 and MDAMB361 cells (Fig. 3C–F). Specifically, exposing tumor cells to both CD36 ligands determines the activation of initiator caspases 8 and 9, which triggers executioner caspases 3 and 7 (Casp-3/7) and results in cell lysis and altered cellular processes. We found that **11**, with a lower CD36 binding affinity than **13** (Fig. 1), exerted significant apoptotic activity on both HER2 + BC cell lines starting after 72 h of treatment at the higher concentration tested (50 μM; Fig. 3C,E). Conversely, **13**, with greater CD36 binding affinity (Fig. 1), was active on both cell targets at all tested time points (Fig. 3D,F).

11 and 13 inhibit FA uptake in HER2 + BC cells

CD36 mediates the transport of LCFAs, such as palmitic acid (C16:0), into cells, thereby promoting saturated FA uptake and utilization for tumor viability and progression. To examine whether the observed antiproliferative effects on HCC1569 and MDAMB361 cells were related to the ability of the ligands to impair the intracellular internalization of FA, both target cell lines were incubated with **11** or **13** (25 μM), with DMSO as a control and C16:0. We assessed the total lipid profile, as esterified FAs, showing that both hits led to a significant reduction in the C16:0-fold increase (FI) in HCC1569 and MDAMB361 cells (Fig. 4) after C16:0 supplementation. Taken together, these results demonstrate that our two CD36 binders also inhibit FA uptake. It is important to note that the relationship between CD36 expression levels and inhibitory efficacy may be influenced by additional cellular factors. As reported by Åbacka et al.[27]a similar potency for a CD36-targeting compound was observed across cell lines with differing CD36 expression, suggesting that the inhibitor activity is not solely dependent on CD36 abundance.

Anti-tumor effects of CD36 and HER2 dual blockade

Owing to the well-established role of CD36 in cancer progression and resistance to anticancer therapy[16,17,21,28], we investigated the antitumor effects mediated by concomitant inhibition of CD36 and HER2 in HCC1569 cells, which express the highest level of CD36.

Firstly, HCC1569 cells were incubated for 48 h, 72 h, or 96 h with two concentrations of **11** and **13** (12.5 μM and 25 μM), or with high concentration of lapatinib (7.2 μM)[34]; then the effect of the combination of the two inhibitors was tested via an SRB bioassay.

Compared to individual agents tested in a monotherapy setting, the dual blockade of CD36 and HER2 showed an enhanced antiproliferative effect (Fig. 5A–D), although the experiments were not designed to quantitatively assess synergistic interactions. These results reveal the possibility of using CD36 inhibitors to potentiate the anticancer effects mediated by lapatinib, and potentially by other anti-HER2 agents currently used as standard-of care therapies.

Modeling the interaction of 11 and 13 within the CD36 binding site

The in silico docking search identified **11** and **13** as the best predicted binders of CD36. The best affinity of hit **11** (3-[(4-anilinophenyl)carbamoyl]phenyl] acetate, MW 346.4) was displayed by just three poses over 80 (3/80, $\Delta G = -10.1$ kcal/mol) in the structural cluster, whereas most poses were located at the surface of the protein. In its best pose, most of **11** is buried inside the protein upper cavity (Fig. 6A) and surrounded by hydrophobic residues (including Leu140, Leu187, Val389, Leu391 and Leu200, but also Arg337 and Lys334); its phenyl acetate moiety points toward the solvent, exchanging H-bonds with the hydroxyl group of Tyr149 (2.8 Å) and with the main chain amine of Thr195 (3.3 Å; Fig. 6A,B).

The best two poses for hit **13** (3-[3-(4-benzoylphenoxy)propyl]-4(3 H)-quinazolinone, MW 384.4) (2/80, $\Delta G = -10.3$ kcal/mol) are similar to those observed for **11**, with most of its structure buried inside the cavity interacting with hydrophobic residues (Leu140, Leu187, Val198, Leu200 and Arg337), and with the buried benzoyl group establishing an H-bond with Gly199 (2.8 Å; Fig. 6A,B). Similar with the acetate group in **11**, the quinazolinone moiety of **13** is directed toward the solvent, exchanging a H-bond with the main chain amine Thr195 (2.8 Å).

To further explore possible interactions of **11** and **13** within CD36, we performed two molecular dynamic simulations of the extracellular domain of CD36 in presence of both selected hits. We started from the best binding pose obtained for each ligand by in silico docking, and after system equilibration, the two productive runs lasted for 250 ns.

Cluster analysis of **11** (g_cluster, cutoff 0.08) showed an early stabilization of the compound (after 35 ns) in a location slightly below the docking site (~6 Å down shift), with its phenyl acetate moiety pointing toward the solvent between loop 195–204 and alpha helix 331–334 (Fig. 6C). The root mean square fluctuation (r.m.s.f.) of **11** after 35 ns is ~0.5 Å, with a higher mobility for the external phenyl acetate group of ~1 Å. The reference conformation of **11** in the cluster (at 210 ns) is stabilized mostly by hydrophobic interactions (Leu200, Ile330, Ile341, Val339, and Val389) and by two H-bonds between the carbamoyl group and Arg337 side chain and Tyr202 carbonyl main chain (Fig. 6C).

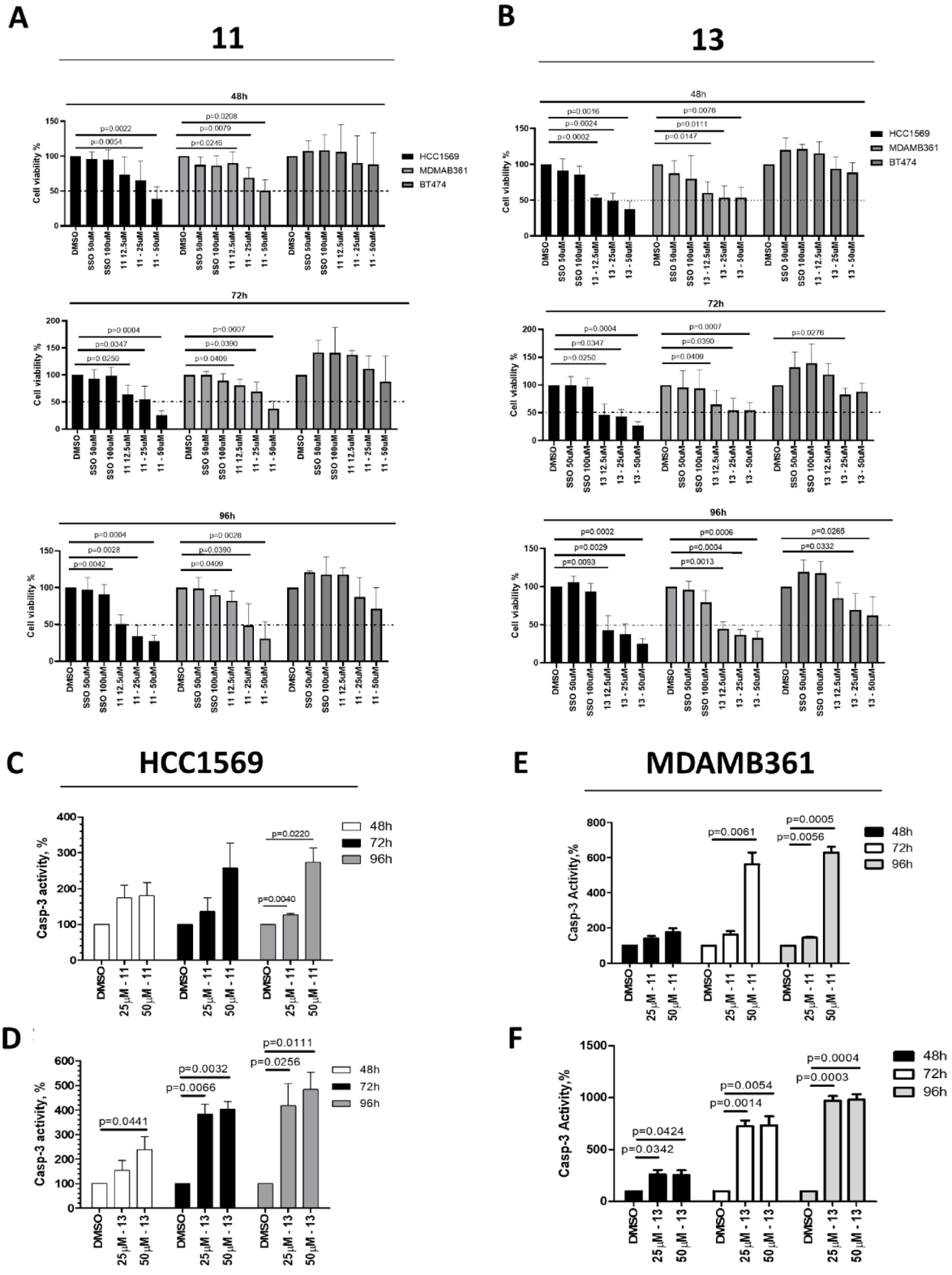

Fig. 3. Cytotoxic activity and apoptotic cell death of HER2 + BC cells upon exposure to 11 and 13. (**A**) Cytotoxic activity of **11** and (**B**) of **13** anti-CD36 hit compounds on HCC1569, MDAMB361 and BT474 cells incubated with SSO; tested at 50 μM and 100 μM, and **11** and **13** hits tested at 12.5 μM, 25 μM, 50 μM, for different time intervals (48 h, 72 h and 96 h), respectively; and subsequently evaluated by the cytotoxic SRB bioassay. Data are presented as the means ± SEMs ($n = 3–5$). Significance was calculated using a two-tailed paired t test. (**C**) and (**D**) Apoptotic activity (Casp-3) of HCC1569 cells, and (**E**) and (**F**) of MDAMB361 cells evaluated after exposure to **11** (upper panel) and **13** (lower panel) CD36 inhibitors at 25 and 50 μM for different times (48 h, 72 h and 96 h), respectively. Data are presented as the means ± SEMs ($n = 3$). Significance was calculated by using a two-tailed paired Student's t test.

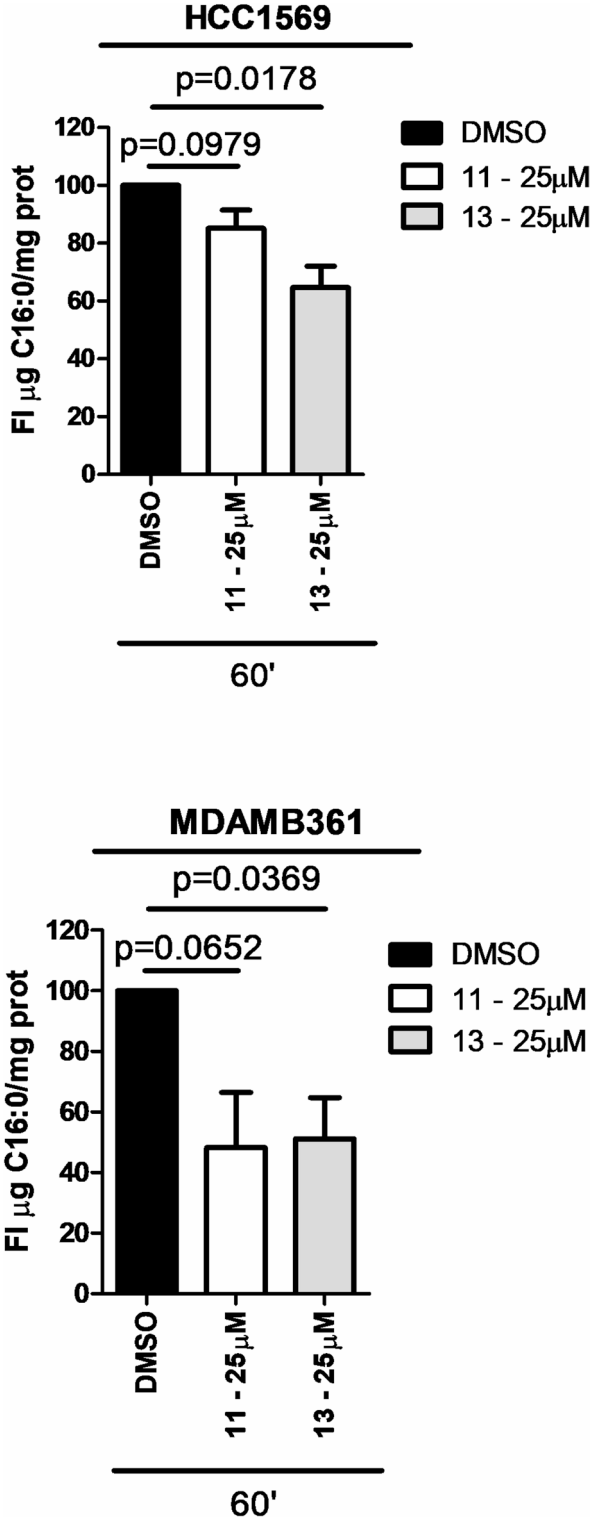

Fig. 4. FA uptake in HER2 + BC cell lines treated with hit compounds 11 and 13. HCC1569 (upper) and MDAMB361 (lower) cells were incubated with **11** and **13** (25 µM) for 60 min in the presence of palmitic acid conjugates with bovine serum albumin. FA uptake was assessed using gas chromatography-flame ionization detector (GC-FID) analysis. Data are presented as fold increase (FI) values (treatment versus control) calculated from the normalized C16:0 content. Results are presented as the means ± SEMs ($n = 3$). Significance was determined using a two-tailed paired Student's t test.

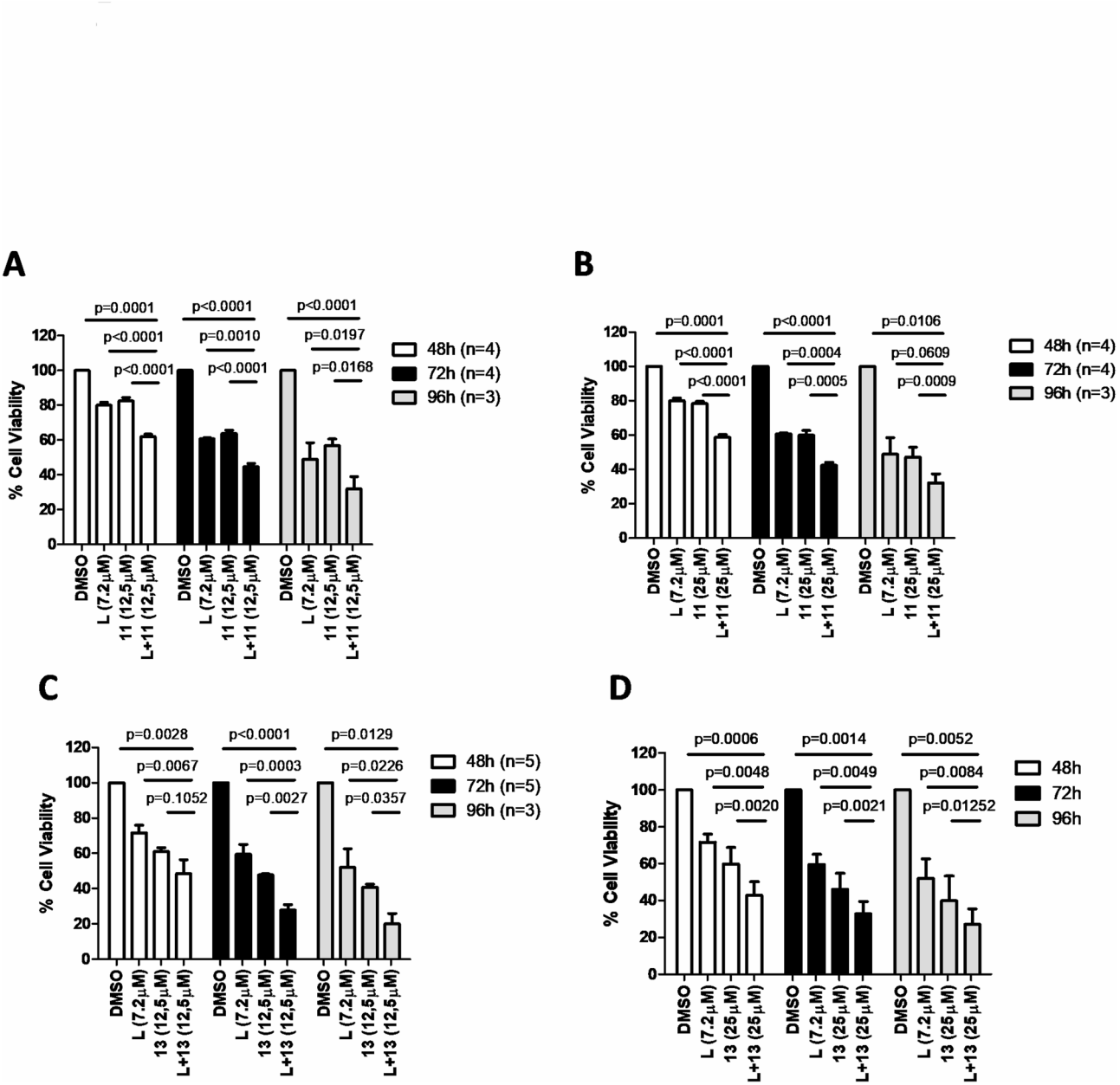

Fig. 5. Tumor proliferation of HCC1569 cells after treatment with lapatinib, 11 or 13 tested as a monotherapy and in combination with the anti-HER2 agent. (**A**–**D**) Proliferation of HCC1569 cells after exposure to lapatinib (7.2 μM), **11** or **13** CD36 inhibitors (12.5 μM and 25 μM) alone or in combination, as evaluated by SRB assay. HCC1569 cells were incubated with **11** tested at (**A**) 12.5 μM or (**B**) 25 μM, or with **13** tested at (**C**) 12.5 μM or (**D**) 25 μM alone or in combination for 48–72 h. Results are presented as the mean ± SEM ($n = 3/4$). Significance was calculated using a two-tailed paired t test.

Overall, throughout the entire simulation, the hydrogen bond between the carbonyl main chain of Tyr202 and the carbamoyl amine of **11** was stable (81% of the simulation time), while hydrogen bonds between the main chain carbonyl of Leu200 and the anilinophenyl nitrogen (18%), and between Arg337 and the carbamoyl carbonyl (8%) were less stable. Finally, one of the benzene rings in the anilinophenyl group is involved in aromatic-cation interaction with Lys334.

Cluster analysis (0.08 cutoff) showed that **13** stabilized early (after 29 ns) in a location completely buried inside the protein channel at ~12 Å from the docking site. The central conformation of the cluster (at 220 ns) is stabilized mostly by hydrophobic interactions and by H-bonds with main chains of Arg337 and Gly199 and with the side chain of Arg63 (Fig. 6D). Overall, during the entire simulation, the hydrogen bond between the carbonyl group in **13** and Arg435 was quite persistent (60%), whereas the interactions involving Arg337 (21%) and Gly199 (26%) were less stable.

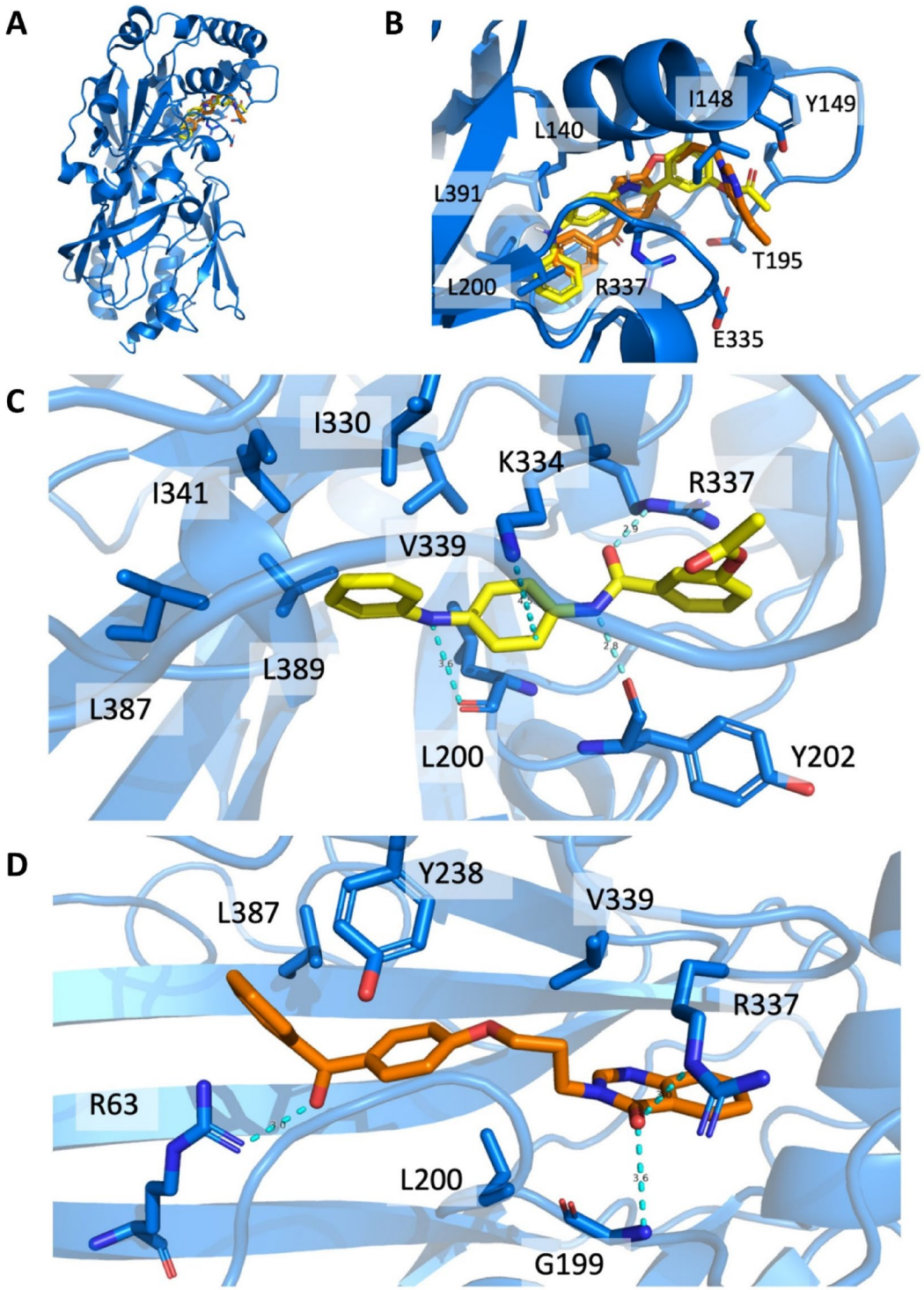

Fig. 6. Modeling of the interaction between 11 and 13 and CD36. (**A**) in silico docking of **11** (sticks with yellow carbon atoms) and **13** (sticks with orange carbon atoms) with CD36 (blue cartoons); (**B**) same as (**A**) with a closer view (selected CD36 amino acids in sticks with blue carbon atoms); (**C**) central cluster conformation of **11** during the MD simulation (at 210 ns); (**D**) central cluster conformation of **13** during the MD simulation (at 220 ns). Figures were prepared with PyMol (http://www.pymol.org/).

Hits **11** and **13** share common features and different characteristics, which can be used to perform structural optimization along two parallel routes. For both ligands, the buried diphenyl moieties can be elongated, considering the size of the internal protein cavity. On the other hand, while the hydrophilic head of **11** impedes the molecule from penetrating the protein channel, **13** can penetrate the CD36 core completely, allowing for further modifications. Notably, inside the cavity that hosts both molecules, the presence of Cys333 can be used

to develop covalent inhibitors. In general, our structural information will be useful for guiding the optimization of **11** and **13** to improve their binding affinity to CD36 and their bioavailability/pharmacological profile.

Discussion

Solid preclinical studies highlighted that HER2 + BC is a neoplastic disease with a lipogenic phenotype, as it is highly addicted to an exacerbated need of FA to proliferate, survive and progress. Remarkably, the key lipogenic enzyme FASN is strongly overexpressed/activated in HER2 + BC and is associated with poor clinical outcome[9,42]. In this context, a PFL of reciprocal stimulation between HER2 and FASN, which couples lipid biosynthesis with the oncogenic signaling, has been revealed[9]. Accordingly, the existence of this oncometabolic circuit strongly implies that pharmacological HER2 inhibition could be sufficient per se to inhibit also FASN, thus activating FA uptake as an adaptive metabolic response.

The rewiring of FA uptake via the CD36 translocase plays a key role in predicting therapeutic resistance and poor prognosis in both HER2 + BC preclinical models during acquisition of lapatinib resistance[21] and in clinical setting of HER2 + BC treated in neo-adjuvant setting with anti-HER2 drugs[16,22]. In particular, the findings emerging from the study by Ligorio F et al.[16], which showed the association between higher baseline intratumor CD36 gene expression levels and poorer patient outcome in both HER2 + BC neoadjuvant clinical trials NeoALTTO[43] and NeoSphere[44], suggest that the activation of the FA uptake as compensatory metabolic pathway in presence of lapatinib-mediated HER2 inhibition can be extended also to the humanized anti-HER2 antibodies trastuzumab and pertuzumab, that have different mechanisms of action versus TKI. In this metabolic scenario, our study addresses and validates the question of the potential efficacy of HER2 and CD36 dual blockade as a valid metabolism-based combinatorial therapeutic strategy to potentiate the activity of anti-HER2 agents in HER2 BC resistant to targeted therapy[22].

The experimental investigation of the CD36 receptor as a novel therapeutic target in oncology is limited by the lack of CD36 specific inhibitors, suitable for in vivo applications. The possible use of the irreversible, aspecific CD36 inhibitor SSO in preclinical experiments has intrinsic limitations. In fact, SSO (200 μM) is able to block FA uptake by approximately 65%; its binding to CD36 lysine 164[26] could be negatively affected by acidic pH, which is a peculiar trait of the cancer microenvironment, and its specificity for CD36 is debatable since SSO interacts with other cytoplasmic proteins that affect intracellular FA metabolism[45]. Other nanomolar inhibitors for the cellular uptake of both ox-LDL and LCFAs[46], i.e. AP5055 and AP5258, have been reported, however no data are available on their direct interaction with CD36 or other cell proteins. Conversely, the recently identified compound SMS121 has been shown to bind CD36 with high affinity and to inhibit FA uptake, as assessed using BODIPY-C12 in acute myeloid leukemia cell lines (KG-1 and THP-1). Interestingly, SMS121 exhibited a similar efficacy (IC_{50} ~160 μM) in both cell lines, despite their differing CD36 expression levels. This observation suggests that additional cellular mechanisms may contribute to the inhibitory effect observed, beyond CD36 inhibition alone[27].

In this work, using the crystal structure of the extracellular domain of CD36, we screened in silico a commercial library of small molecules for their ability to interact with a FA binding cavity of the protein[29]. The 15 best-ranked ligands were experimentally tested, allowing for the selection of **11** and **13.** Both compounds are able to bind CD36 with higher affinity than SSO and with increased ability to impair FA internalization. These novel CD36 ligands decreased per se HER2-resistant HER2 + BC cells proliferation index, inducing cell death by apoptosis.

Moreover, treatment of HER2 + BC cells with hits **11** and **13** in combination with the anti-HER2 TKI lapatinib significantly increases antitumor activity, providing a promising future approach to target HER2-positive BC cells resistant to HER2-targeted therapy.

Conclusions

This study revealed the identification of two novel hit compounds selectively targeting CD36, the transmembrane FA transporter involved in their intracellular uptake, which recently emerged as a potentially new and targetable metabolic biomarker predictive of resistance to anti-HER2 therapies. Our in vitro findings provided evidence of the activity of the two selected CD36 inhibitors that can be further optimized into therapeutic tools to improve anti-HER2 therapy efficacy in the lipogenic HER2 + BC disease, thus representing an ideal combinatorial metabolic approach to boost targeted therapy efficacy in treatment-refractory HER2 + BC patients.

Data availability

All the data related to this study are available within the articleThe datasets used and/or analysed during the current study available from the corresponding author on reasonable request.

Received: 17 January 2025; Accepted: 1 August 2025
Published online: 06 August 2025

References

1. Sung, H. et al. Global cancer statistics 2020: GLOBOCAN estimates of incidence and mortality worldwide for 36 cancers in 185 countries. *CA Cancer J. Clin.* **71**, 209–249 (2021).
2. Loibl, S. & Gianni, L. HER2-positive breast cancer. *Lancet* **389**, 2415–2429 (2017).
3. Vernieri, C. et al. Resistance mechanisms to anti-HER2 therapies in HER2-positive breast cancer: current knowledge, new research directions and therapeutic perspectives. *Crit. Rev. Oncol. Hematol.* **139**, 53–66 (2019).
4. Hanahan, D. Hallmarks of cancer: new dimensions. *Cancer Discov.* **12**, 31–46 (2022).
5. Santos, C. R. & Schulze, A. Lipid metabolism in cancer. *FEBS J.* **279**, 2610–2623 (2012).

6. Pascual, G., Domínguez, D. & Benitah, S. A. The contributions of cancer cell metabolism to metastasis. *Dis. Model. Mech* **11**, (2018).
7. Gámez-Chiachio, M., Sarrió, D. & Moreno-Bueno, G. Novel therapies and strategies to overcome resistance to Anti-HER2-Targeted drugs. *Cancers (Basel)* **14**, (2022).
8. Menendez, J. A. et al. Inhibition of fatty acid synthase (FAS) suppresses HER2/neu (erbB-2) oncogene overexpression in cancer cells. *Proc. Natl. Acad. Sci. U. S. A.* **101**, 10715–10720 (2004).
9. Menendez, J. A. & Lupu, R. Fatty acid synthase and the lipogenic phenotype in cancer pathogenesis. *Nat. Rev. Cancer*. **7**, 763–777 (2007).
10. Jin, Q. et al. Fatty acid synthase phosphorylation: a novel therapeutic target in HER2-overexpressing breast cancer cells. *Breast Cancer Res.* **12**, R96 (2010).
11. Kuo, C. Y. & Ann, D. K. When fats commit crimes: fatty acid metabolism, cancer stemness and therapeutic resistance. *Cancer Commun. (Lond).* **38**, 47 (2018).
12. Wang, J. & Li, Y. CD36 Tango in cancer: signaling pathways and functions. *Theranostics*. **9**, 4893–4908 (2019).
13. Guerrero-Rodríguez, S. L., Mata-Cruz, C. & Pérez-Tapia, S. M. & Velasco-Velázquez, M. A. Role of CD36 in cancer progression, stemness, and targeting. *Front. Cell. Dev. Biol.* **10**, (2022).
14. Hale, J. S. et al. Cancer stem cell-specific scavenger receptor CD36 drives glioblastoma progression. *Stem Cells*. **32**, 1746–1758 (2014).
15. Ladanyi, A. et al. Adipocyte-induced CD36 expression drives ovarian cancer progression and metastasis. *Oncogene*. **37**, 2285–2301 (2018).
16. Ligorio, F. et al. Predictive role of CD36 expression in HER2-Positive breast cancer patients receiving neoadjuvant trastuzumab. *J. Natl. Cancer Inst.* **114**, 1720–1727 (2022).
17. Pascual, G. et al. Targeting metastasis-initiating cells through the fatty acid receptor CD36. *Nature*. **541**, 41–45 (2017).
18. Abumrad, N. A. et al. Cloning of a rat adipocyte membrane protein implicated in binding or transport of long-chain fatty acids that is induced during preadipocyte differentiation. Homology with human CD36. *J. Biol. Chem.* **268**, 17665–17668 (1993).
19. Liang, Y. et al. CD36 plays a critical role in proliferation, migration and tamoxifen-inhibited growth of ER-positive breast cancer cells. *Oncogenesis*. **7**, 98 (2018).
20. Gyamfi, J. et al. Interaction between CD36 and FABP4 modulates adipocyte-induced fatty acid import and metabolism in breast cancer. *NPJ Breast Cancer*. **7**, 129 (2021).
21. Feng, W. W. et al. CD36-Mediated metabolic rewiring of breast cancer cells promotes resistance to HER2-Targeted therapies. *Cell. Rep.* **29**, 3405–3420e5 (2019).
22. Castagnoli, L. et al. CD36 enrichment in HER2-positive mesenchymal stem cells drives therapy refractoriness in breast cancer. *J. Exp. Clin. Cancer Res.* **44**, 19 (2025).
23. Tzeng, S. F. et al. PLT012, a humanized CD36-Blocking antibody, is effective for unleashing antitumor immunity against liver cancer and liver metastasis. *Cancer Discov.* **OF1–OF21** https://doi.org/10.1158/2159-8290.CD-24-1409 (2025).
24. Watt, M. J. et al. Suppressing fatty acid uptake has therapeutic effects in preclinical models of prostate cancer. *Sci. Transl. Med.* **11**, (2019).
25. Harmon, C. M., Luce, P., Beth, A. H. & Abumrad, N. A. Labeling of adipocyte membranes by sulfo-N-succinimidyl derivatives of long-chain fatty acids: Inhibition of fatty acid transport. *J. Membr. Biol.* **121**, 261–268 (1991).
26. Kuda, O. et al. Sulfo-N-succinimidyl oleate (SSO) inhibits fatty acid uptake and signaling for intracellular calcium via binding CD36 lysine 164. *J. Biol. Chem.* **288**, 15547–15555 (2013).
27. Åbacka, H. et al. SMS121, a new inhibitor of CD36, impairs fatty acid uptake and viability of acute myeloid leukemia. *Sci. Rep.* **14**, 9104 (2024).
28. Ruan, C., Meng, Y. & Song, H. CD36: an emerging therapeutic target for cancer and its molecular mechanisms. *J. Cancer Res. Clin. Oncol.* **148**, 1551–1558 (2022).
29. Hsieh, F. L. et al. The structural basis for CD36 binding by the malaria parasite. *Nat. Commun.* **7**, 12837 (2016).
30. Trott, O. & Olson, A. J. AutoDock vina: improving the speed and accuracy of Docking with a new scoring function, efficient optimization, and multithreading. *J. Comput. Chem.* **31**, 455–461 (2010).
31. Morris, G. M. et al. AutoDock4 and AutoDockTools4: automated Docking with selective receptor flexibility. *J. Comput. Chem.* **30**, 2785–2791 (2009).
32. García-García, C. et al. Dual mTORC1/2 and HER2 Blockade results in antitumor activity in preclinical models of breast cancer resistant to anti-HER2 therapy. *Clin. Cancer Res.* **18**, 2603–2612 (2012).
33. Zazo, S. et al. Generation, characterization, and maintenance of trastuzumab-resistant HER2 + breast cancer cell lines. *Am. J. Cancer Res.* **6**, 2661–2678 (2016).
34. O'Neill, F. et al. Gene expression changes as markers of early lapatinib response in a panel of breast cancer cell lines. *Mol. Cancer*. **11**, 41 (2012).
35. Li, H., Black, P. N. & DiRusso, C. C. A live-cell high-throughput screening assay for identification of fatty acid uptake inhibitors. *Anal. Biochem.* **336**, 11–19 (2005).
36. Koschorke, A. et al. Phenethyl isothiocyanate hampers growth and progression of HER2-positive breast and ovarian carcinoma by targeting their stem cell compartment. *Cell. Oncol. (Dordr).* **42**, 815–828 (2019).
37. Nava Lauson, C. B. et al. Linoleic acid potentiates CD8 + T cell metabolic fitness and antitumor immunity. *Cell. Metab.* **35**, 633–650e9 (2023).
38. Galli, G. et al. Circulating fatty acid profile as a biomarker for immunotherapy in advanced Non-Small cell lung cancer. *Clin. Lung Cancer*. **23**, e489–e499 (2022).
39. Páll, S., Abraham, M. J., Kutzner, C., Hess, B. & Lindahl, E. Tackling exascale software challenges in molecular dynamics simulations with GROMACS. *Lect Notes Comput. Sci.* **8759**, 3–27 (2015).
40. Schmid, N. et al. Definition and testing of the GROMOS force-field versions 54A7 and 54B7. *Eur. Biophys. J.* **40**, 843–856 (2011).
41. Malde, A. K. et al. An automated force field topology builder (ATB) and repository: version 1.0. *J. Chem. Theory Comput.* **7**, 4026–4037 (2011).
42. Bueno, M. J. & Colomer, R. A. Fatty acid synthase inhibitor shows new anticancer mechanisms. *EBioMedicine*. **2**, 778–779 (2015).
43. Baselga, J. et al. Lapatinib with trastuzumab for HER2-positive early breast cancer (NeoALTTO): a randomised, open-label, multicentre, phase 3 trial. *Lancet*. **379**, 633–640 (2012).
44. Gianni, L. et al. Efficacy and safety of neoadjuvant Pertuzumab and trastuzumab in women with locally advanced, inflammatory, or early HER2-positive breast cancer (NeoSphere): a randomised multicentre, open-label, phase 2 trial. *Lancet Oncol.* **13**, 25–32 (2012).
45. Jay, A. G., Simard, J. R., Huang, N. & Hamilton, J. A. SSO and other putative inhibitors of FA transport across membranes by CD36 disrupt intracellular metabolism, but do not affect FA translocation. *J. Lipid Res.* **61**, 790–807 (2020).
46. Geloen, A. et al. CD36 inhibitors reduce postprandial hypertriglyceridemia and protect against diabetic dyslipidemia and atherosclerosis. *PLoS One*. **7**, e37633 (2012).

Acknowledgements

We would like to thank Mrs. Cristina Ghirelli for her excellent technical assistance, and Mrs. Mameli for her

secretarial assistance.

Author contributions

Conceptualization: L.C., M.M., and S.M.P.; Resources: M.M., and S.M.P.; Data curation: L. C., F.B., M.B., P.T., P.A.C., G.G., A.F., P.C., V.R., M.M., and S.M.P.; Formal analysis: L.C., F.B., M.B., P.T., P.A.C., G.G., A.F., P.C., V.R., C.C., F.L., C.V., D.A P.S., E.T.; Supervision: M.M., and S.M.P.; Validation: L.C., and F.B.; Investigation: L.C., F.B., P.A.C., and M.M.; Methodology: L.C., F.B., M.B., P.T., P.A.C., G.G., A.F., P.C., V.R.; Project administration: S.M.Pupa; Funding acquisition: L.C., M.M, and S.M.P; Writing-original draft: L.C, M.M, and S.M.P; Writing - review & editing: L.C, F.B, M.B, P.T, P.A.C, G.G, A.F, P.C; V.R, C.C, A.M.R, F.L, C.V, P.S, D.A, E.T, E.M., M.M., and S.M.P. All authors reviewed the manuscript.

Funding

This study was funded by a grant from the Associazione Italiana Ricerca Cancro (AIRC) call 2019 Id#22943 P.I. Serenella M. Pupa and partially co-funded by the Italian Ministry of Health "Ricerca Corrente". We acknowledge support for A. Franceschini (2021–2023), F. Boni (6 months-2022), P. Cocomazzi (6 months-2022), C. Capuzzoni (2023–2024) and M. Bigliardi (2024–2025) as recipients of a fellowship from AIRC call 2019 Id#22943. We acknowledge additional support for L. Castagnoli as a recipient of a fellowship from Fondazione Veronesi (Call 2023) and from Fondazione Pezcoller (Call 2022). Mario Milani thanks the Italian Consortium "Cineca" (https://www.hpc.cineca.it/) for supercomputing resources allocated to the project *IsCa7_drp* 2023–2024.

Declarations

Competing interests

C. Vernieri reports research grants from Roche (to the Institution); Role in Advisory Boards or consultancies: Eli Lilly; Novartis; Pfizer; Daiichi Sankyo; Menarini Stemline; Astra Zeneca. Honoraria as a speaker: Eli Lilly; Novartis; MSD; Pfizer, Istituto Gentili; Menarini Stemline; Accademia Nazionale di Medicina; F. Ligorio reports Honoraria as a speaker from Novartis, Pfizer, Eli-Lilly, Accademia di Medicina. No competing interests were declared by the other authors.

Additional information

Supplementary Information The online version contains supplementary material available at https://doi.org/10.1038/s41598-025-14639-z.

Correspondence and requests for materials should be addressed to M.M. or S.M.P.